Composite Structures 86 (2008) 154–164

Contents lists available at ScienceDirect

Composite Structures

journal homepage: www.elsevier.com/locate/compstruct

Towards the robotic characterization of the constitutive response of composite materials

John G. Michopoulos [a,*], John C. Hermanson [b], Tomonari Furukawa [c]

[a] Center for Computational Material Science, Special Projects Group, Code 6390.2, Computational Multiphysics Systems Laboratory, US Naval Research Laboratory, Washington, DC 20375, United States

[b] USDA Forest Service Forest Products Laboratory, Engineered Wood Properties and Structures, Madison, WI, United States

[c] Cooperative Research Centre for Advanced Composite Structures, School of Mechanical and Manufacturing Engineering, University of New South Wales, Sydney, Australia

ARTICLE INFO

Available online 13 March 2008

Keywords:
Mechatronic characterization
Material constitutive response
Automated characterization
Multidimensional loading spaces
Parameter identification
Data-driven characterization

ABSTRACT

A historical and technical overview of a paradigm for automating research procedures on the area of constitutive identification of composite materials is presented. Computationally controlled robotic, multiple degree-of-freedom mechatronic systems are used to accelerate the rate of performing data-collecting experiments along loading paths defined in multidimensional loading spaces. The collected data are utilized for the inexpensive data-driven determination of bulk material non-linear constitutive behavior models as a consequence of generalized loading through parameter identification/estimation methodologies based on the inverse approach. The concept of the dissipated energy density is utilized as the representative encapsulation of the non-linear part of the constitutive response that is responsible for the irreversible character of the overall behavior. Demonstrations of this paradigm are given for the cases of polymer matrix composite materials systems. Finally, this computational and mechatronic infrastructure is used to create conceptual, analytical and computational models for describing and predicting material and structural performance.

Published by Elsevier Ltd.

1. Introduction

The present paper aims in reporting on how computational technologies along with computational modeling in conjunction with mechatronic technologies, have evolved through the years and especially recently in order to facilitate the constitutive characterization of polymer matrix composite (PMC) materials. Special emphasis will be given to recent developments related to completing the construction of a third generation system that has been undertaken under the "Application of Dissipated Energy density to comPosite sTructures" (ADEPT) research program that has been recently initiated under funding from the US Office of Naval Research (ONR).

The need to be able to predict the behavior of continuous systems under complex generalized loading conditions is primarily driven from the need to design and utilize such systems in various areas of human technological endeavors. The means of addressing this need through the ages has been generally encapsulated by an approach that seeks the development continuous system modeling within the context of continuum mechanics. Successful models have been traditionally considered to be those that can faithfully and accurately reproduce actual (usually experimentally established) behavior of existing systems.

The contemporary demands for cost and time reduction, multimission design requirements, and increased systemic complexity resulting from the need for realistic systems predictive simulation (usually resulting in very computation intensive mathematical models), constitute the technology-push motivators for automation of research. On the other hand, the innate human tendency for satisfying curiosity and for engineering elegance and efficient solutions that solve problems both on a societal or/and a personal scale, along with the rampant but predictable [1–3] evolution of computational and other associated technologies are the primary science pull motivators for attempting to automate the research process in general and its application to composites in particular.

An important thesis of the present work is that there are two major areas where researchers might look for improving the ability to produce better, faster and cheaper products that except for a very few cases worldwide, have not been recognized widely as areas of opportunity. One is the realization of the role of the researcher relative to the scientific method and the exploitation of the available intellectual, computational and physical resources. The other is the distinct enormous potential of the computational technology and other associated with it technologies. In the past we have presented some elements of a computational epistemology of scientific method as it relates to the constitutive

* Corresponding author.
E-mail addresses: john.michopoulos@nrl.navy.mil (J.G. Michopoulos), jhermans@wisc.edu (J.C. Hermanson), t.furukawa@unsw.edu.au (T. Furukawa).

0263-8223/$ - see front matter Published by Elsevier Ltd.
doi:10.1016/j.compstruct.2008.03.009

characterization of materials in order to ground for the epistemologic lineage of the approach that was pioneered by researchers at the Naval Research Laboratory (NRL) [3].

This paper follows with a brief historical overview of the state of affairs regarding the 6 degree-of-freedom (DoF) mechatronic technology evolution as the core technology behind a systematically automated methodology for identifying the constitutive behavior of composites. The subsequent section introduces the system theoretic view of the general structural and material system with an emphasis on the black box input–output relation and its differential equation system specification. The role of the optimizer relative to the physical system, its analytical model and an experimental framework that serves as data-generator and as system behavior observation apparatus are underlined. In the sub-section that follows, an equivalent system decomposition that isolates the role of the constitutive behavior sub-system is presented. This is achieved by pursuing the generalized hyperelastic pseudo-potential approach in the context of the Galerkin projection of the differential operator corresponding to the partial differential equation derived from the conservation of momentum. The subsequent sub-section describes a brief taxonomy of the kinds of models that can be constructed to analytically represent the behavior of both the overall black box system representation or the constitutive response sub-system behavior in particular. The heart of the paper is the next section that describes the planned experimental and computational procedure. In particular, the specimen geometry, the loading and material space sampling and the dissipated energy density considerations along with the description of the inverse problem solved to determine it are given. The final section of this work presents a short discussion and conclusions with an emphasis on the new role that can be played by the researcher-designer as it applies to the utilization of data-driven robotic identification of material behavior relative to the formation of failure criteria and their exploitation.

2. Overview of 6-DoF robotic systems for material characterization

The industrialized-deductive scientific method in order to achieve high reliability behavioral prediction [1–3], requires acquiring massive amounts of facts in the form of experimental data. This suggests that a capability to amplify the natural human ability to perform experiments is necessary. In this spirit, mechanical, hydraulic, electric, and computational power (in the form of robotic systems) have been combined to amplify not only the human ability for deforming material specimens, but also the ability to gather and process multiple sensor data faster than the duration of an actual complete experiment. The degree of automation employed in material testing through the combination of computational and testing machine technologies has evolved extensively in the last 40 years. Mechatronic testing machines were developed to achieve industrial rates of acquisition of observations about material behavior.

For a more detailed exposition of the evolution of systems used for material constitutive behavior identification with less or equal to 3 DoF see [3–5]. Here we will only present the evolution of our efforts as they relate to 6 DoF systems because of their relevance to our current activities.

In order to address issues of large specimens, with combined in and out of plane loading a series of 6 DoF testing machines was developed at NRL. The first version used six actuators with analogue controlled valves, mounted on an I-beam frame referred to as NRL66.1. This machine was designed, built and tested in 1983 (see Fig. 1a). A robotic arm was used to insert and remove specimens. Both data acquisition and control processes were increased to 6 DoF. These were the three translations and three rotations applied by the movable (lower) grip on the one edge of the specimen. The large open frame of this machine allowed actuators to be placed parallel to three orthogonal axes to simplify the algebraic representation of the kinematics of the movable grip.

Starting in 1993, yet another new 6 DoF loader system (6DLS) was designed and constructed at NRL (see Fig. 1b) referred to as NRL66.2. It was built-in a hexapod architecture configuration developed originally for flight simulator platforms (Stewart platform) and it is classifiable as a 6–6p parallel robotic mechanism. The hexapod architecture made the machine more compact, far stiffer (less prone to energy storage by deformation of the machine itself), and easier to disassemble for modification or relocation than the previous machine.

The movable grip in this case was the upper one and was attached to the movable 3-armed star-shaped base of the system.

In 1996, the original analogue controlled actuators of the prototype machine were replaced with longer stroke, digitally controlled actuators with minimal changes needed in other structural parts of the machine. This system will be referred to as NRL66.3. This system was never completed due to funding discontinuities and its construction has been recently restarted with an entirely new design specification and multiphysics excitation requirements. This

a b
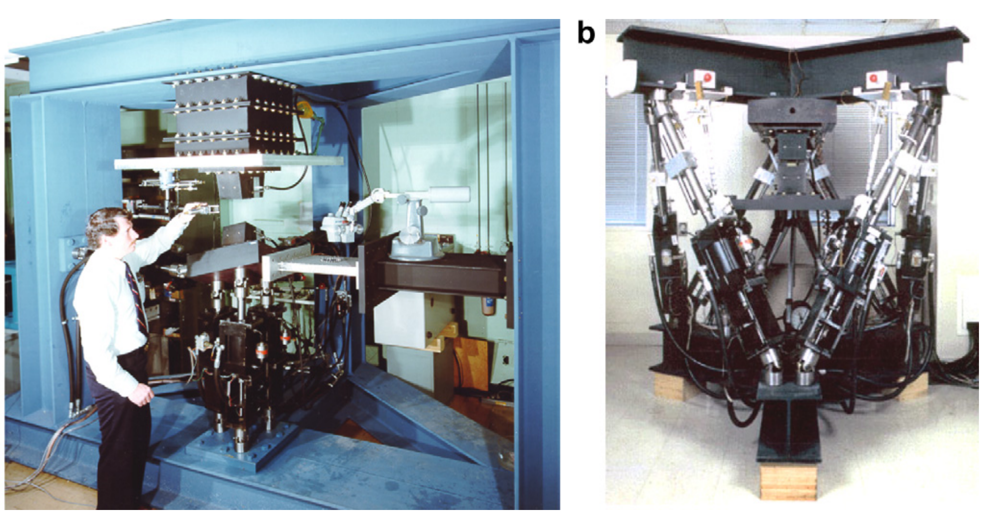

Fig. 1. NRL66.1 (a) and NRL66.2 (b) 6-DoF robotic testing systems.

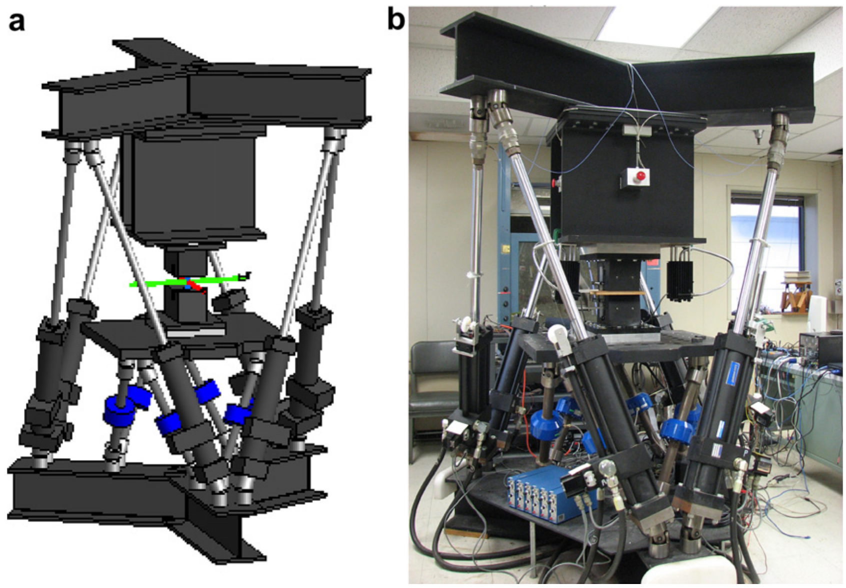

Fig. 2. 3D geometry model of NRL66.3 (a) and image of current state of it (b).

system is under construction with emphasis on the mechanical loading primarily for the needs of the ADEPT program. It will also feature an automated specimen feeding device, a wireless sensor network infrastructure, and for the first time it will employ a whole-field 3D optical method for measuring the displacement and strain fields on the surface of the specimen. It is scheduled to be completed within 2008.

A 3D model of its geometry is shown Fig. 2a. A view of the current construction phase of the system is shown in Fig. 2b.

This is a system that has been designed to evolve to the fourth generation of testing machines; a multidimensional generalized loader system (MDGLS) in that additional capability for measuring non-mechanical conjugate pairs of material state variables will be added. This affords the opportunity of using the loader to identify physical systems under the simultaneous action of thermal, electromagnetic, substance diffusion, and mechanical loading effects in order to facilitate data-driven formation of behavioral models for the respective materials and structures.

In addition to NRL's efforts, the Forest Products Laboratory in Madison Wisconsin has built its own hexapod configuration system for the purpose of characterizing natural composites such as wood, and wood plastic composites. This system will be referred to as FPL66 and it can be seen in Fig. 3. A significant difference of FPL66 compared to NRL66.x systems is that instead of being built completely from scratch (as all NRL systems), it exploited the built-in technology of a system by Rexroth–Hydraudyne Inc. that was originally built for flight simulation/amusement platforms. Collaborative efforts between NRL and FPL will take advantage of this system as secondary system to be used for characterization of polymer matrix composites as well.

3. Systemic perspective of a structural system

3.1. The input–output relation black box

The phenomenological characterization of any system behavior is always based on the Baconian [6] setting of observing the system from the outside and attempting to establish a model representation of its behavior by establishing an input–output relation. As shown in Fig. 4, the general procedure we have been promoting and following involves the determination of a system model based on the generalized design optimization idea of minimizing the error between the measured behaviors of the actual system and the system model under construction. This is occurring while an experimental frame controls the input excitation of both the

Fig. 3. Forest products laboratory FPL66 system.

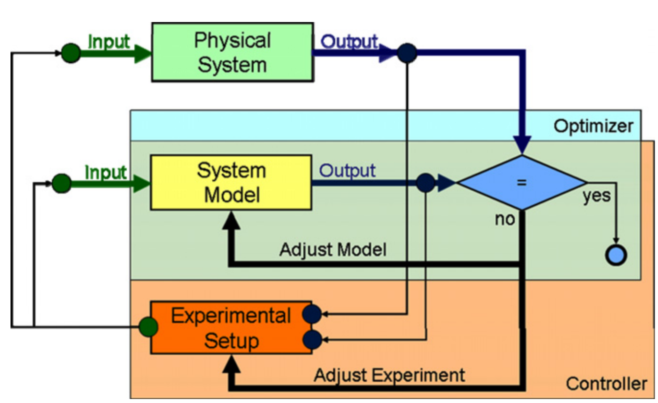

Fig. 4. Process of identifying the model of a physical system via an experimental frame.

physical system and its model and at the same time it measures the inputs and the outputs. While the optimizer section of the diagram is responsible for adjusting the form of system model so its outputs match the physical system outputs, the controller section is responsible for adjusting aspects of the experimental setup behavior under the same conditions and under a frozen representation of the system model. In this context determination of the system model is the activity of a system identification that for the case of a continuum structural system amounts to the structural behavior identification and eventually the characterization of the constitutive response of the material system involved. Since this activity is data-driven (based on the behavior data of the systemic response acquired by the experimental frame) and leads into the model determination, it belongs to a special category of inverse problems.

The main objective of our effort in the present paper is to both demonstrate the most important formal and experimental aspects of this process, we begin with the formal aspects first.

When the system model under construction is characterized by the continuous behavior of both the input and output then we can borrow the differential equation system specification (DESS) from the theory of modeling and simulation [7] to formally describe the abstraction of the system model. Accordingly, the DESS of the system model can be described as the 6-tuple structure:

$$\mathrm{DESS} = \langle T, X, Y, Q, f, \lambda \rangle, \tag{1}$$

where the time base set is a subset of the set of real numbers $T \subseteq \Re$, and the real-valued vector spaces $X \subseteq \Re^m, Y \subseteq \Re^n, Q \subseteq \Re^p$ of dimensions m, n, p, respectively define the input, output and state sets; $f{:}Q \times X \to Q$ is the rate of state change function; $\lambda{:}Q \to Y$ (Moore-type) or $\lambda{:}Q \times X \to Y$ (Mealy-type) is the output function. The necessary condition for the existence of a unique well-defined state trajectory determined for every state and input, is expressed by the Lipschitz condition stated as

$$\|f(q,x) - f(q',x)\| < k\|q - q'\| \tag{2}$$

for all $q, q' \in Q$, and input values $x \in X$, where k is a constant and $\|\cdot\|$ is the Euclidian norm.

In the context of the inverse problem setting, the challenge at hand is the determination of Q, f, λ when X, Y are known. For continuous Mealy-type systems where the rate of state change is identity (like in the case of linear elastic systems) all is needed to be determined is the output function $\lambda(x)$. Similarly, for Moore-type systems the output function can be taken to be the identity function and therefore only the state change function needs to be determined. Both of these types of problems can be covered by the so called input/output relation observation (IORO) specification as it is defined by the theory of modeling and simulation [7] that defines the association morphism between the inputs and the outputs vectors. As is shown by the definitions of Eq. (1), this is given by the composition $\mathbf{g}(\boldsymbol{q},\boldsymbol{x}) = \mathbf{f} \circ \boldsymbol{\lambda} = \boldsymbol{y}$. For the case of DESS, the y_i components of the output vector $\boldsymbol{y}$ are expected to be the solutions of a set of n coupled ordinary differential equations of the form:

$$\sum_{j=1}^{r} a_j \frac{\mathrm{d}^j}{\mathrm{d}t^j} y_i(t) = f_i(y_1(t), \ldots, y_n(t), x_1(t), \ldots, x_m(t)) \quad \text{for } i = 1, \ldots, n, \tag{3}$$

where r is the order of the highest time derivative and a_j are the corresponding weighting coefficients. In this case the specification is called multiDESS. Since the essential behavior of the system is encapsulated by this representation, reaching the desired outcome (for the forward problem) of determining the y_n outputs as function of the x_m inputs involves the integration of this system. In many practical cases, the system of Eq. (3) can be reduced to a system of algebraic equations expressed in the general form by

$$\mathbf{Fy} = \mathbf{x}, \tag{4}$$

that can be solved by inversion of the behavior array $\mathbf{F}$ if it is square ($n = m$), or by applying a pseudo-inversion methodology like singular value decomposition if $\mathbf{F}$ is rectangular ($n > m$) for the case when Eq. (4) represents and overdetermined system. In the inverse problem setting, $\mathbf{F}$ needs to be determined when $\mathbf{y}$, $\mathbf{x}$ are known.

For the case of a continuum structural system, usually the behavior of the system is encapsulated by some partial differential equation (PDE) governing the evolution of some dependant variable representing a scalar field or a component of a vector or tensor field that, in addition to time, depends on the spatial coordinates as they play the role of additional (to time) independent variables. It has been shown repeatedly [8,9] that once the continuous scalar field is projected into a discrete space through a projection operator that corresponds to the values of the field on the points of a discrete grid distributed in the spatial domain and bounded by the surface boundary of the structural material, the problem of solving the PDE is reduced to the problem of solving a system like that of Eq. (3). This is usually the approach followed by the various finite element formulations [8,9].

3.2. Systemic decomposition equivalence

A general representation of the equations that govern a physical problem over a region of space V can be written as:

$$Lu = P \tag{5}$$

where u and P are, respectively the unknown and the "loading" fields, while L is a differential operator.

A projection $\tilde{u}$ of the field u on an appropriate vector space of basis functions $\{G_i\}$ – that can generally be piecewise polynomials of space coordinates – can be represented as

$$\tilde{u} = \sum_i q_i G_i. \tag{6}$$

This projection must satisfy the weak form of Eq. (5) given by:

$$\forall \phi \in E \quad \int_V \phi(L\tilde{u} - P)\mathrm{d}V = 0, \tag{7}$$

where E is a functional space. The choice of E leads to different approximation methods. For example, according to the widely spread Galerkin method [8,9] ϕ is chosen as a linear combination of the G_i's according to:

$$\phi \in E_{\mathrm{Galerkin}} \iff \phi = \sum_i \phi_i G_i \tag{8}$$

The form of ϕ_i is chosen so that ϕ satisfies the homogeneous version of the boundary conditions prescribed for $\tilde{u}$.

When the differential operator is linear, or after the necessary linearization (if it is non-linear), and having discretized the domain to a collection of elements N, our approximate problem takes the form of a linear system in the q_i that can be written as:

$$\sum_i^N q_i \int_V \phi L G_i \mathrm{d}V = \int_V \phi P \mathrm{d}V \tag{9}$$

This linear system is usually expressed in the matrix form:

$$\mathbf{Kq} = \mathbf{F} \tag{10}$$

Thus, solution of the discretized problem, at this point, is equivalent to inverting the matrix $\mathbf{K}$. The similarity of this equation to Eq. (4) ensures that this system is a special form of that given by Eq. (4). However, in order to address the decomposition between material and the total structural behavior we need to identify the internal structure of $\mathbf{K}$.

For many materials their constitutive behavior when they are under mechanical deformation conditions can be expressed by:

$$\boldsymbol{\sigma} = \boldsymbol{\sigma}(\boldsymbol{\varepsilon}) \tag{11}$$

Since our system unknowns are expressed in terms of the displacement component fields we need one of the strain measure definitions to associate the strain with the displacement fields. In the general case we can just write:

$$\boldsymbol{\varepsilon} = \boldsymbol{\varepsilon}(\mathbf{u}) \tag{12}$$

Since the stress and the strain are energy conjugate tensor fields the principle of virtual work permits the expression:

$$\mathbf{K}_{ij} = \int_V \left(\frac{\partial}{\partial q_i} \quad \sigma_{kl} \frac{\partial \varepsilon_{kl}}{\partial q_j} \right) dV \tag{13}$$

The product rule of differentiation it can be applied to yield:

$$\mathbf{K}_{ij} = \int_V \left(\frac{\partial \sigma_{kl}}{\partial q_i} \frac{\partial \varepsilon_{kl}}{\partial q_j} + \sigma_{mn} \frac{\partial^2 \varepsilon_{mn}}{\partial q_i \partial q_j} \right) dV \tag{14}$$

Another use of the chain rule enables the expression:

$$\frac{\partial \sigma_{kl}}{\partial q_i} = \frac{\partial \sigma_{kl}}{\partial \varepsilon_{\mu\nu}} \frac{\partial \varepsilon_{\mu\nu}}{\partial q_i}, \tag{15}$$

that when substituted in Eq. (14) yields:

$$\mathbf{K}_{ij} = \int_V \left(\frac{\partial \varepsilon_{\mu\nu}}{\partial q_i} \frac{\partial \sigma_{kl}}{\partial \varepsilon_{\mu\nu}} \frac{\partial \varepsilon_{kl}}{\partial q_j} + \sigma_{mn} \frac{\partial^2 \varepsilon_{mn}}{\partial q_i \partial q_j} \right) dV \tag{16}$$

This expression shows dependence of $\mathbf{K}_{ij}$ on the quantity $\frac{\partial \sigma_{kl}}{\partial \varepsilon_{\mu\nu}}$ that expresses the material response in terms of its multidimensional tangent modulus. For the case of an elastic system this tangent modulus coincides with Hooke's elastic fourth order tensor $C_{kl\mu\nu} = \frac{\partial \sigma_{kl}}{\partial \varepsilon_{\mu\nu}}$. In order to establish a more intimate appreciation of the meaning behind the effect of the material behavior on the stiffness matrix $\mathbf{K}_{ij}$ we consider the internal energy density (per unit volume) on hyperelastic materials. In this case the internal energy density is identical to the strain energy density given by

$$U = \int_0^{\varepsilon} \boldsymbol{\sigma}(\boldsymbol{\varepsilon}) d\boldsymbol{\varepsilon} \tag{17}$$

As an example we consider the case of a purely linear elastic material where Eq. (11) can be written in the form

$$\sigma_{kl} = C_{kl\mu\nu} \varepsilon_{\mu\nu} \tag{18}$$

that when introduced in Eq. (17) yields

$$U = \frac{1}{2} \sigma_{kl} \varepsilon_{\mu\nu} = \frac{1}{2} C_{kl\mu\nu} \varepsilon_{kl} \varepsilon_{\mu\nu} \tag{19}$$

A intrinsic property of all hyperelastic materials (and the special case of elastic ones) is the existence of a potential permitting the generation of stresses according to

$$\sigma_{kl} = \frac{\partial U}{\partial \varepsilon_{kl}} \tag{20}$$

When this relation is applied to Eq. (19) recovers identically Eq. (18) as expected. Introducing Eq. (19) into Eq. (20) and differentiating a second time with respect to the strain components yields the tangent modulus in the form

$$\frac{\partial \sigma_{kl}}{\partial \varepsilon_{\mu\nu}} = \frac{\partial^2 U}{\partial \varepsilon_{kl} \partial \varepsilon_{\mu\nu}} = C_{kl\mu\nu} \tag{21}$$

Substituting the left equality of this relation into the expression (16) yields

$$\mathbf{K}_{ij} = \int_V \left(\frac{\partial \varepsilon_{\mu\nu}}{\partial q_i} \frac{\partial^2 U}{\partial \varepsilon_{kl} \partial \varepsilon_{\mu\nu}} \frac{\partial \varepsilon_{kl}}{\partial q_j} + \sigma_{mn} \frac{\partial^2 \varepsilon_{mn}}{\partial q_i \partial q_j} \right) dV \tag{22}$$

The implication of this relation is that systemic behavior can be considered now as the composition of the material behavior given by Eq. (21) and the spatial behavior expressed by the rest of the terms in Eq. (22). Thus, to characterize the system here means to characterize the material, which in turn means to identify the internal strain energy density function. In the case of an elastic material this is equivalent to the determination of the constants that are elements of Hooke's tensor $C_{kl\mu\nu}$.

What used to be a "black box" to be identified according to Fig. 5a, has now been reduced to a gray box where some part of it is known and some is still unknown according to Fig. 5b.

It is worthwhile noting here that the effect of changing the material now is only an input of the material behavior black box, while the effect of changing the shape of the structure is an input of the structural behavior (green box in Fig. 5b).

3.3. Taxonomy of data-driven models

The problem of determining an analytical representation for the gray element of Fig. 5b from its inputs and outputs belongs to the family of system identification problems and many methods are available to be employed for this purpose.

A short and not all inclusive taxonomic classification of the models that are possible to be constructed is shown in Fig. 6. The class-diagram semantics of inheritance and generalization within the context of the universal modeling language (UML) [10] have been utilized to capture a coarse classification of this kind. Arrows indicate the direction of generalization or abstraction (inverse to inheritance). The class with the tip of the arrow attached to it represents the generalization or the parent (in terms if inheritance) of the class that the root of the arrow is attached on. Thus specialization evolves from left to right and generalization from right to left in Fig. 6.

At the first level of abstraction we have the explicit, implicit and hybrid models. Explicit are considered all those models where the mathematical formulas used to connect the dependent with the independent state variables of a constitutive model are originating from a physically describable model. All involved parameters can be identified within the area of the physical space of the model at hand. Examples of explicit constitutive models are all those based on energy functions formulated from the inner products of the state variables or equivalent thermodynamic potentials based on Legendre transformation of the internal energy function of the materials. In this case constitutive equations are produced via the differentiation of these functions with respect to the independent state variables and produce expressions for the dependent ones. Models in this case include the classical elasticity,

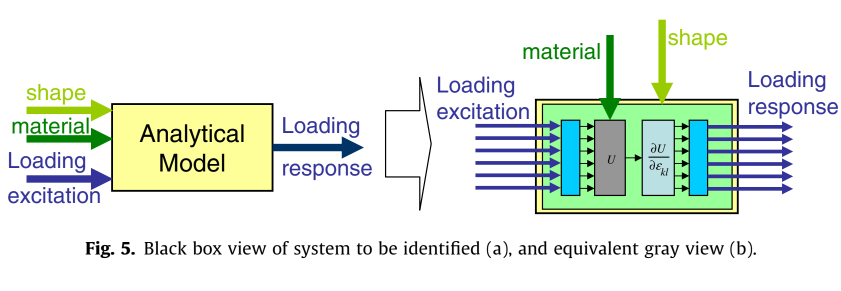

Fig. 5. Black box view of system to be identified (a), and equivalent gray view (b).

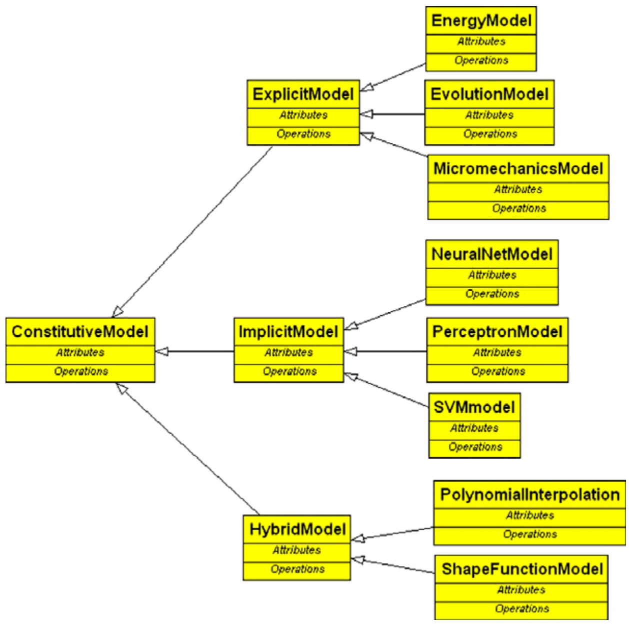

Fig. 6. Taxonomic classification of constitutive models.

hyperelasticity and other load-path independent multi-field theories. Other approaches in this category are based on modeling of the continuum at lower length scale that of the continuum such as the micro- and the meso-scales with the addition of an arbitrary composition behavior. This category would include all micromechanics and mesomechanics models.

Implicit models are those that are completely agnostic to the physics and assume many possible mathematical representations that are blind to the physical parameterization of the system at hand except for state variables. Examples of implicit constitutive models are all those that ignore the internal physical view of the system and only consider its input and output state variables. Thus any machine-learning or input–output associating technology would belong in this category. Examples are artificial neural networks (ANNs), multilayered perceptrons (MLPs), support vector machines (SVMs), etc.

Hybrid models are all those exhibiting characteristics from both of the previous cases. Since any representation for systemic behavior can be considered as a composition of the sub-models of sub-behaviors, it is then expected that it is possible for some of these sub-models to have explicit and some to have implicit nature. Thus a constitutive model that implements an arbitrary polynomial function as a sum of basis functions for the energy of the system would belong to this category because it still considers continuum mechanics premises (i.e. it accepts the existence of an internal potential energy for the material) but at the same time it does not enforce a highly specialized version of this polynomial in a manner that satisfies frame reference transformation invariance (that would require it to be a function of the state variable invariants) and in that way is implicit.

It is important to realize here that all these model representations regardless of the category they belong are particular points in the global model space.

4. Experimental and computational procedure

The role of NRL66.3 is to serve as a data-generator for identifying the material response. It has been made to automate control of the rigid body motion of the boundary of the specimen that is held by the movable grip and at the same time measure the boundary displacements and tractions at the grips, and the whole-field strain distributions. The 6–6p architecture of the actuators of the NRL66.3 allows it to move in a manner that the resulting motion involves 6 DoFs relative to any frame of reference. The motivation for this 6-dimensional excitation is based on the anticipation that all possible combinations of loading are expected to generate the widest possible variations of the strain tensor components and thus will excite the constitutive system shown in Fig. 5b in a manner that will force the model under construction to be aware of them. This will allow the recovered constitutive model to be able to reproduce them consistently.

4.1. Specimen geometry

The typical flat specimen geometry is shown in Fig. 7 where the dark gray areas indicate the part of the specimen that is placed into the grips, and the light gray area is the area that deforms under the influence of the applied loading. The double notches on the specimen are introduced to disturb the strain field and to ensure that some areas of the specimen (not necessarily near the notch tips) will experience non-linear constitutive response due to the corresponding strain fields. Any geometrical feature that could have this effect would be acceptable in our formulation. However, the notches are very economic and practical from a specimen manufacturing perspective and this was the main reason motivating this selection.

Assuming that the lower grip stays fixed during the experiments, the upper grip has the capability to apply 6 DoF motion that amount to applying three translations t_x, t_y, t_z and three rotations r_x, r_y, r_z.

An arbitrary grip motion can always be resolved into these six basis components as shown in Fig. 8 and are referred to a frame of reference attached at the center of the specimen, and three rotations about the axes of the same system. The color contours on Fig. 8 represent the magnitudes of total displacement fields for Fig. 8a–c, respectively and the magnitudes of the total rotation vector fields for Fig. 8d–f, respectively. They were produced by running a representative finite element analysis (FEA) for each of the boundary conditions corresponding by each one of the loading cases specified in Fig. 8.

Clearly, these 6 basis cases implicitly define a 6-dimensional loading space that contains any possible paths that can excite the

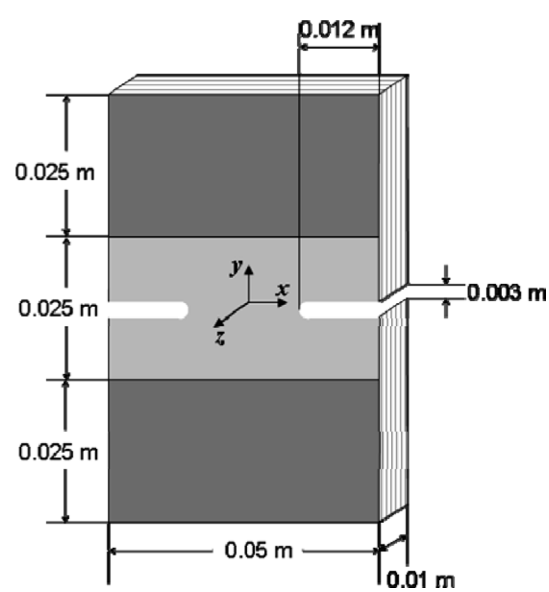

Fig. 7. Typical geometry of NRL66.3 specimen.

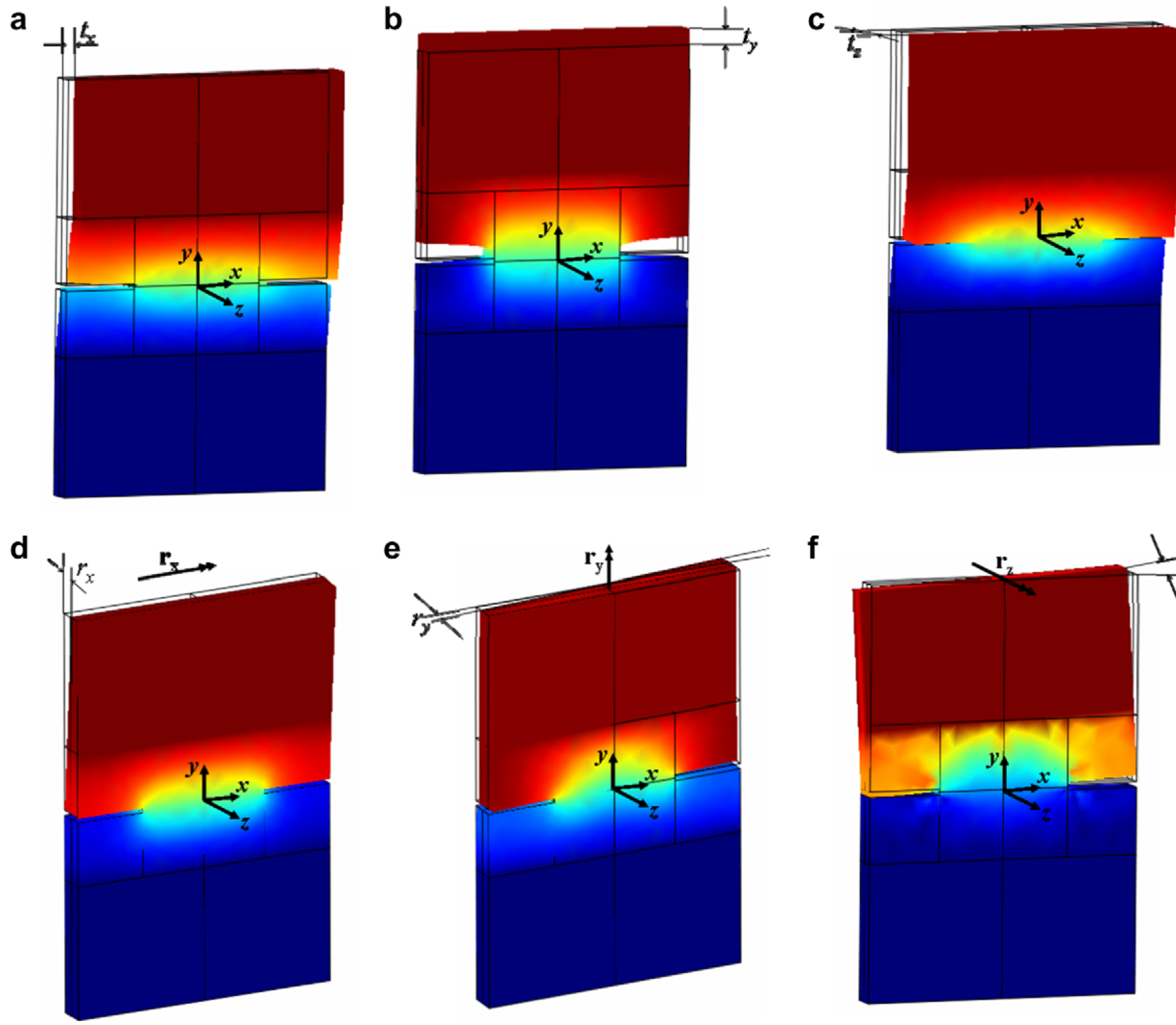

Fig. 8. The six basis cases associated with each DoF of the motion applied by NRL66.3 on the movable grip: translation along x-axis (a), translation along y-axis (b), translation along z-axis (c), rotation about x-axis (d), rotation about y-axis (e) and rotation about z-axis (f).

specimen system and consequently will generate the corresponding set of strain states that will be used to determine the bulk constitutive response of the material system.

If these are the loading excitation components, then the corresponding response of the system can be described in terms of the reaction forces f_x, f_y, f_z and moments m_x, m_y, m_z. Therefore, the measuring system of the NRL66.3 is designed to acquire all 6 + 6 = 12 measurements corresponding to both groups of these quantities (i.e. 6 controlled kinematic inputs defining the motion of the specimen and pose of the movable grip, and the corresponding 6 reaction quantities.

For the sake of representational and dimensional homogeneity we introduce the two column arrays

$$u = (u_1, u_2, u_3, u_4, u_5, u_6)^{\mathrm{T}} = (t_x, t_y, t_z, r_x \cdot 1m, r_y \cdot 1m, r_z \cdot 1m)^{\mathrm{T}} \qquad (23)$$

and

$$f = (f_1, f_2, f_3, f_4, f_5, f_6)^{\mathrm{T}} = (f_x, f_y, f_z, m_x/1m, m_y/1m, m_z/1m)^{\mathrm{T}} \qquad (24)$$

In Eq. (23) the quantities u_4, u_5, u_6 correspond to the displacement at the end of a rigid bar of length 1.0 m connected rigidly to the gripped area of the specimen. Reciprocally, the quantities f_4, f_5, f_6 represent the corresponding reaction forces at the end of this rigid bar. This transformation is based on the fact that it maintains invariant the inner product of these two arrays that expresses the total work applied into the system according to

$$W = \sum_{i=1}^{6} W_i = \sum_{i=1}^{6} u_i f_i = t_x f_x + t_y f_y + t_z f_z + r_x m_x + r_y m_y + r_z m_z. \qquad (25)$$

Since our intension is to expose the identification system to the most representative set of strain states, the question becomes how to sample the 6-dimensional space spanned by the bases formed by the components of u. This is the problem of proper sampling of the excitation space.

4.2. Loading space sampling

The plan that we have followed in the past exploited the path-independence of polymer matrix composites and adopted a policy of sampling the excitation space with proportional paths distributed evenly across the observation space. We have shown recently, that for the case of entirely elastic responses, we can employ a methodology that identifies optimal continuous paths in the loading space in a manner that best determines the unknown elements of the anisotropic Hooke's elasticity tensor involved in describing the linear elastic behavior of anisotropic composites [11–13]. Since this technique has not been extended to the non-linear case yet (though in progress), we will continue pursuing the uniform sampling of the loading space with loading proportional paths.

In order to define the loading paths in terms of their proportions as a function of the space dimensionality and their density per unit of surface they cross, we pursue the generalization of the 3 DoF case. This case would correspond to the in-plane loading as it has been shown in the past [5,14,15]. For a loading situation that is realistic for shell-like structures the only relevant components of u would be u_1, u_2, u_6. This consideration implies the existence of 3-dimensional subspace spanned by these components as the corresponding basis vectors. In Fig. 9a this space is presented along with a unit cube. Any tiling of this space by multiple occurrences of this cube (or other polyhedra) has the property that all lines (paths) starting from the origin and crossing the vertices and midpoints of the edges and midpoints of the faces of the first unit cube also pass from corresponding points of adjacent cubes. Such a regular tiling of the 3-space creates a uniform distribution of the loading paths. However, it is more convenient from an analytic representation perspective to describe these paths in terms of the points lying on the projections of the characteristic points of the cube on a sphere centered at the origin as shown in Fig. 9a. This involves utilizing the spherical coordinate system transformation. Fig. 9b shows three successive increments of the loading paths (black lines), the corresponding points sampled (red, green and blue points) and the truncated spherical shells where all these points lie on.

According to this scheme the space is sampled by commanding NRL66.3 to follow radial proportional paths and acquire data at the points that these paths intersect concentric spheres. The term proportional path here means that every path i when represented as a vector starting in the origin and ending at point j, can be resolved to its components in the (u_1, u_2, u_6) frame according to

$$\mathbf{p}_i^j = p_{i1}^j\mathbf{u}_1 + p_{i2}^j\mathbf{u}_2 + p_{i6}^j\mathbf{u}_6 \quad (26)$$

where $p_{i1}^j, p_{i2}^j, p_{i6}^j$ are the magnitudes of each component, and furthermore

$$p_{ik}^j = r_i^j a_{ik}^j, k \in \{1, 2, 6\} \text{ with } a_{ik}^j = a_{ik}^{j+1}. \quad (27)$$

For the 3-dimensional space of Fig. 9b it is known from the spherical to Cartesian transformation that

$$p_{i1}^j = r_i^j \cos(\varphi_1^i) p_{i2}^j = r_i^j \sin(\varphi_2^i)\cos(\varphi_1^i),$$
$$p_{i3}^j = r_i^j \cos(\varphi_2^i)\cos(\varphi_1^i) \quad (28)$$

where $\varphi_1^i \in [0, \pi], \varphi_2^i \in [0, 2\pi]$ are the angles of the declination from the vertical axis, and the unfolding angle on the equatorial plane, respectively. Comparing Eqs. (27) and (28) yields that

$$a_{i1}^j = \cos(\varphi_1^i), a_{i2}^j = \sin(\varphi_2^i)\cos(\varphi_1^i), a_{i6}^j = \cos(\varphi_2^i)\cos(\varphi_1^i) \quad (29)$$

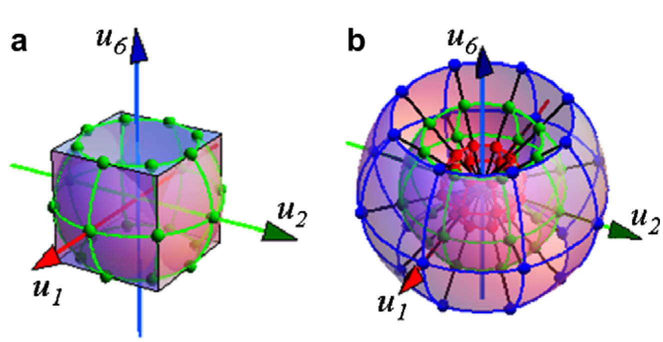

Fig. 9. Sampling of 3-space according to cubic tiling (a) and expanding sphere surface (b).

The spacing of the sampled points on the surface of the sphere centered at the origin of the (u_1, u_2, u_6) frame has been determined by taking the intersections of 8 equally spaced meridians (along the equator on the u_1, u_2 plane) at $\varphi_1^i = n\pi/4, n = 0, \ldots, 7$, and intersecting them 2 parallel circles and the equator at $\varphi_2^i = n\pi/4, n = 1, \ldots, 3$. Thus the number of sampled points will be nsp = 8 × 3 = 24. In this description the number of points along a meridian passing from each of the pole and crossing the equator for just the northern hemisphere was *nep* = 1 and the dimensionality of the space was $n = 3$.

In order to be able to generalize this process to dimensions more than three, we employ the concept of the generalization of the sphere to that of the hypersphere [16]. A hypersphere of dimension n is called an n-sphere and denoted as $\mathbf{S}^n$. It is an n-dimensional manifold and can be embedded in a Euclidean $(n + 1)$-space. The space enclosed by the n-sphere is called an $(n + 1)$-ball. Under these considerations the regular sphere is 2-sphere embedded in a 3-dimensional space and it encloses a 3-ball.

We can now define a coordinate system in an n-dimensional Euclidean space which is analogous to the spherical coordinate system defined for the 3-dimensional Euclidean space, in which the coordinates consist of a radial coordinate r_i^j, and $n - 1$ angular coordinates $\varphi_1^i, \varphi_2^i, \ldots, \varphi_{n-1}^i$. Then the corresponding Cartesian coordinates expressing the projections of the loading path on the n axes of the Cartesian frame will be given by [16],

$$\begin{aligned}
p_{i1}^j &= r_i^j \cos(\varphi_1^i) \\
p_{i2}^j &= r_i^j \sin(\varphi_1^i)\cos(\varphi_2^i) \\
p_{i3}^j &= r_i^j \sin(\varphi_1^i)\sin(\varphi_2^i)\cos(\varphi_3^i) \\
&\cdots \\
p_{i(n-1)}^j &= r_i^j \sin(\varphi_1^i)\cdots\sin(\varphi_{n-2}^i)\cos(\varphi_{n-1}^i) \\
p_{in}^j &= r_i^j \sin(\varphi_1^i)\cdots\sin(\varphi_{n-2}^i)\sin(\varphi_{n-1}^i)
\end{aligned} \quad (30)$$

Since Eq. (30) is valid for all dimensions it also applies for the $n = 6$ case that corresponds to our full case where all components of kinematic excitation $\{u_1, u_2, u_3, u_4, u_5, u_6\}$ are present.

In the interest of economy, it is imperative that the least number of specimens is used to characterize a material system. In the past we have used one specimen per loading path with very good results. Since it is meaningless to use on specimen for more than one path we will maintain this approach. Therefore for each laminate system we will use as many specimens (at least) as the number of paths used to sample the excitation space.

We have established that the number of paths as a function of the dimension n of the space and the number of *nep* points is given by

$$n_{\text{paths}} = (4 + 4nep)(1 + 2nep)^{n-2} \quad (31)$$

Plotting the number of paths as a function of the dimensions according to Eq. (31) for $n = 2, \ldots, 6$ and for *nep* = 1, 2, 3 demonstrates as shown in Fig. 10 demonstrates how quickly the number of paths increases. In particular for $n = 6$ the number of paths corresponding to *nep* = 1, 2, 3 is 648, 7500, and 38416, respectively. For the case of $n = 4$ the number of paths corresponding to *nep* = 1, 2, 3 is 72, 300, and 784, respectively. The best possibility of the worst case scenario for dimension $n = 6$ is still much higher than the 15 paths used for the in-plane loader (3-DoF) system that was sampling the system in the (u_1, u_2, u_6) subspace only. In that case we dropped 9 out of the 24 points needed for $n = 3$ and *nep* = 1, because of geometry and loading symmetries of these points lie on the half sphere.

If we assume that the constitutive response of the material can be decomposed to the in-plane and out of plane behaviors, in that they are independent from each-other, then all we need to do is to sample the two subspaces (u_1, u_2, u_6) and (u_3, u_4, u_5) separately.

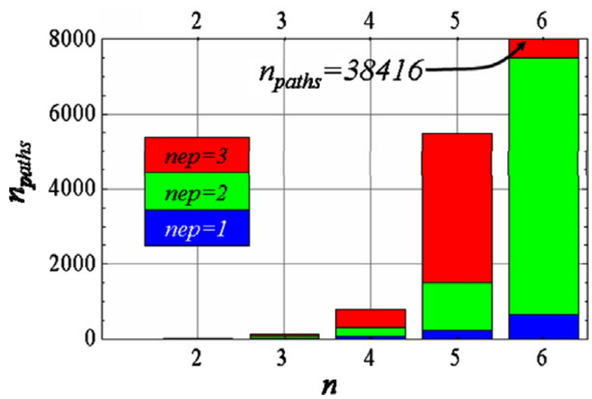

Fig. 10. Number of paths as a function of the space dimension n and *nep*.

Thus, if 15 paths are required for each of these subspaces then the best case scenario could be 15 + 15 = 30 paths.

An intermediate scenario could be based on the fact that the rotation components generate motion on the plane they are normal to. Thus, only four out of the six components can be linearly independent. In this case $n = 4$ and for $nep = 1$ Eq. (31) generates 72 paths.

Whether any of these two path reduction schemes can be acceptable as an issue of research that needs to be confirmed by identifying the material behavior following all of these possibilities and comparing their performance to the general case for $n = 6$.

4.3. Material geometry spaces sampling

As shown in Fig. 5b, the material influences the constitutive response and if our aim is to determine the response of the bulk lamina as opposed to what we test which is a particular laminate, then we need a parameterization that decomposes the lamina from the laminate behavior. For this purpose and in order to maintain low cost we consider obtaining 4 balanced laminate specimen configurations that can be obtained from two balanced laminate plate manufactured productions. Thus by manufacturing balanced laminate plates [±15] and [±30] we can also obtain specimens that can be described as [±75] and [±60] by cutting the specimens out of the original plates in a manner that their y-axis is rotated from the original by 90°. Thus the lamination angle is parameterized according to

$$\theta_L \in [15, 30, 60, 75]^{\circ} \tag{32}$$

In addition, for the case of examining the length scale effects on constitutive behavior one has to address the thickness of the ply, the thickness of the specimen and the specimen dimensions in the x–y plane. Assuming that, as in the case of the lamination angle, we require at least 4 discrete values within the range of the corresponding quantity's parameterization we can now write the formula of the total number of specimens required for a full identification of the material system.

$$n_{\text{spec}} = 2(n_{\text{paths}} \times n_{\theta_L} \times n_{LT} \times n_{Lz} \times n_{Ly} \times n_{Lx}) \tag{33}$$

where $n_{\theta_L}, n_{LT}, n_{Lz}, n_{Ly}, n_{Lx}$ are the numbers indicating the cardinality of the ranges where the lamination angle, the lamina thickness, the specimen thickness, the specimen dimension along y-axis and the specimen dimension along the x-axis, respectively. The coefficient 2 in front of the right hand side of Eq. (33) expresses the desire to repeat every combination at least twice in order to include some redundancy that can help indicating testing anomalies. The overall structure of Eq. (33) clearly indicates that the whole excitation space is the concatenation of the loading path space (3–6 dimensions) with those of additional 5 dimensions associated with the quantities just described. Therefore, the total excitation space will be 3 + 5 = 8 to 6 + 5 = 11 dimensional. This is assuming that we have chosen not to parameterize the shape of notches. Since NRL66.3 will be also measuring the 3 to 6-dimensional loading specification at a number of n_{pp} points per path and the corresponding reaction forces for each combination of the excitation space, and n_{f} particular field quantities (like the components of strain) at n_{op} observation points then the total number of data points acquired for each system will be

$$n_{\text{points}} = n_{\text{npp}} \times [(n_{\text{spec}} + n_{\text{paths}}) + n_{\text{spec}} \times n_{\text{op}} \times n_{\text{f}}] \tag{34}$$

Realistic values in both Eqs. (33) and (34), under the most conservative numerical assumptions, lead to very large values that clearly justify the industrial character of this robotic approach.

It is essential here to indicate that parameterization of the specimen geometry is not going to be applied due to the scope of this effort that requires derivation of an energy density per unit of volume function that is not anticipated to be effected from length scale variations along the x and y directions.

5. Internal energy density considerations

One of the core ideas of our approach is based on the postulate of an additive decomposition of the internal energy density function to a recoverable part $\Theta(\boldsymbol{\varepsilon})$ reflecting (in most cases) the elastic convex potential and a non-recoverable (dissipated) part $\Phi(\boldsymbol{\varepsilon})$ reflecting a dissipative pseudo-potential, according to

$$U(\boldsymbol{\varepsilon}) = \Theta(\boldsymbol{\varepsilon}) + \Phi(\boldsymbol{\varepsilon}) \tag{35}$$

Introducing the usual quadratic elastic energy density

$$\Theta(\boldsymbol{\varepsilon}) = \frac{1}{2}\mathbf{C} : \boldsymbol{\varepsilon} : \boldsymbol{\varepsilon} \tag{36}$$

and the dissipated energy density (DED) function

$$\Phi(\boldsymbol{\varepsilon}) = -\frac{1}{2 + \deg \mathbf{D}(\boldsymbol{\varepsilon})}\mathbf{D}(\boldsymbol{\varepsilon}) : \mathbf{C} : \boldsymbol{\varepsilon} : \boldsymbol{\varepsilon}, \tag{37}$$

where $\mathbf{C}$ is the initial fourth order Hooke's tensor and $\mathbf{D}(\boldsymbol{\varepsilon})$ is a fourth order softening due to damage tensor. Introducing Eqs. (36) and (37) into Eq. (35) yields

$$U(\boldsymbol{\varepsilon}) = \frac{1}{2}\mathbf{C} : \boldsymbol{\varepsilon} : \boldsymbol{\varepsilon} - \frac{1}{2 + \deg \mathbf{D}(\boldsymbol{\varepsilon})}\mathbf{D}(\boldsymbol{\varepsilon}) : \mathbf{C} : \boldsymbol{\varepsilon} : \boldsymbol{\varepsilon}. \tag{38}$$

The gradient of this expression yields the constitutive response

$$\boldsymbol{\sigma} = \frac{\partial U(\boldsymbol{\varepsilon})}{\partial \boldsymbol{\varepsilon}} = \mathbf{C} : \boldsymbol{\varepsilon} - \mathbf{D}(\boldsymbol{\varepsilon}) : \mathbf{C} : \boldsymbol{\varepsilon} = (\mathbf{I} - \mathbf{D}(\boldsymbol{\varepsilon})) : \mathbf{C} : \boldsymbol{\varepsilon} \tag{39}$$

with $\mathbf{I}$ being the fourth order unit tensor. Eq. (39) is consistent with the continuous damage theory approaches [17–20] where the quantity

$$\mathbf{C}^{eff} = (\mathbf{I} - \mathbf{D}(\boldsymbol{\varepsilon})) : \mathbf{C} \tag{40}$$

represents the effective stiffness tensor. If one assumes that the elastic tensor is known then the problem has been reduced to computing the damage tensor that in general can be represented as a tensor with components of the general form

$$D_{ijkl}(\boldsymbol{\varepsilon}) = \mathbf{c}^{m}_{ijkl} \cdot \boldsymbol{\chi}_m(\boldsymbol{\varepsilon}) \tag{41}$$

where $\mathbf{c}_i, \boldsymbol{\chi}_i(\boldsymbol{\varepsilon})$ contain coefficients depending on the material and basis functions of the strain components chosen arbitrarily. In fact, the entire dissipated energy density Φ can be approximated by any of the models shown in Fig. 6 and in particular by a general linear combination of basis functions according to

$$\Phi(\boldsymbol{\varepsilon}) = \mathbf{c} \cdot \boldsymbol{\chi}(\boldsymbol{\varepsilon}) = c_1\chi_1(\boldsymbol{\varepsilon}) + \cdots + c_n\chi_n(\boldsymbol{\varepsilon}) = c_i\chi_i(\boldsymbol{\varepsilon}) \tag{42}$$

In this form $\mathbf{c}$ represents a vector of material dependant coefficients c_i, and $\boldsymbol{\chi}(\boldsymbol{\varepsilon})$ represents a vector of basis functions $\chi_i(\boldsymbol{\varepsilon})$ that depend only on the components of the strain tensor ε. Eq. (42) can be thought as being an interpolation function that allows evaluation of Φ in a 6D strain space where the values of it are known at discrete points lying at the vertices of a grid embedded in the 6D strain space. Geometrically, it represents a 7-dimensional manifold. Determination of Φ is now equivalent to the determination of $\mathbf{c}$.

The principle of virtual work now suggests that in the absence of kinetic energy the externally applied work W must be compensated by the internal energy change into the system according to

$$\int_V U(\varepsilon)\mathrm{d}V = W \tag{43}$$

where

$$W(\mathbf{u}) = \int_0^{\mathbf{u}} \mathbf{f}\cdot \mathrm{d}\mathbf{s}. \tag{44}$$

Introducing Eqs. (35), (36) and (42) into Eq. (43) yields

$$\int_V \Theta(\varepsilon)\mathrm{d}V + \int_V \Phi(\varepsilon)\mathrm{d}V = \frac{1}{2}\mathbf{C} : \int_V \varepsilon : \varepsilon \mathrm{d}V + \int_V \Phi(\varepsilon)\mathrm{d}V = W \tag{45}$$

Since the first term of the left hand side for this equation represents the recoverable energy, it can be substituted by the recoverable work $\frac{1}{2}\mathbf{f}\cdot\mathbf{u}$ to transform a rewriting of Eq. (45)

$$\int_V \mathbf{c}\cdot\boldsymbol{\chi}(\varepsilon)\mathrm{d}V = \int_0^{\mathbf{u}} \mathbf{f}\cdot \mathrm{d}\mathbf{s} - \frac{1}{2}\mathbf{f}\cdot\mathbf{u} \tag{46}$$

The left hand side of this equation represents an approximation of the total energy dissipated over the entire volume of the specimen while the right hand side represents the same quantity as measured by NRL66.3. Therefore, we can determine the unknown vector $\mathbf{c}$ by forming the residual and considering it an objective function to be minimized according to

$$\min e = D - \int_V \mathbf{c}\cdot\boldsymbol{\chi}(\varepsilon)\mathrm{d}V \tag{47}$$

where

$$D = \int_0^{\mathbf{u}} \mathbf{f}\cdot \mathrm{d}\mathbf{s} - \frac{1}{2}\mathbf{f}\cdot\mathbf{u} \tag{48}$$

By discretizing the volume of the specimen with finite elements indexed by e and reapplying this equation for any distinct load increment p along an arbitrary load-path, Eq. (47) becomes

$$\min e^p = D^p - \sum_{e=1}^{\text{nelems}} c_i\chi_i(\varepsilon_e^p)V_e \tag{49}$$

that equivalently can be written as

$$\min \|e\|_{L_2} = \|\mathbf{d} - [\mathbf{X}]\mathbf{c}\|_{L_2} \tag{50}$$

where the matrices $\mathbf{d}$, $\mathbf{X}$, $\mathbf{c}$ have elements $D^p, X_{ip} = \sum_{e=1}^{\text{nelems}}\chi_i(\varepsilon_e^p)V_e$ and c_i, respectively. Since this system is constructed to be overdetermined by the number of times Eq. (46) is applied along the various loading paths, and since it useful to consider the monotonicity and the positive definitiveness of Φ, the problem can be considered to be a global optimization problem with inequality constraints. A plethora of algorithms are available to use for solving this problem [21–23].

When the c_i unknowns are determined, they are saved in a database for further use in simulating the behavior of the material in geometries of the user's choice. This database can be connected with any FEA code that implements the constitutive law derived by introducing Eq. (42) into Eq. (38) to obtain

$$\boldsymbol{\sigma} = \mathbf{C} : \varepsilon - \mathbf{c}\frac{\partial\boldsymbol{\chi}(\varepsilon)}{\partial\varepsilon} \tag{51}$$

which enables the analysis of any structural geometry made of the characterized material.

6. Simulation-based applications

The DED concept has been applied to many applications that require factual determination of PMC behavior including applications for establishing a metric for simulation-based design and distributed health assessment in aerospace applications [24,25] and smart structures [26]. The great majority of the cases analyzed up to know are based on the in-plane characterization of composites by the 3-DoF in-plane loader and therefore they are all of the type where the structure is shell-like. Many applications in the marine and aerospace industry fall in these two categories. For example, Fig. 11

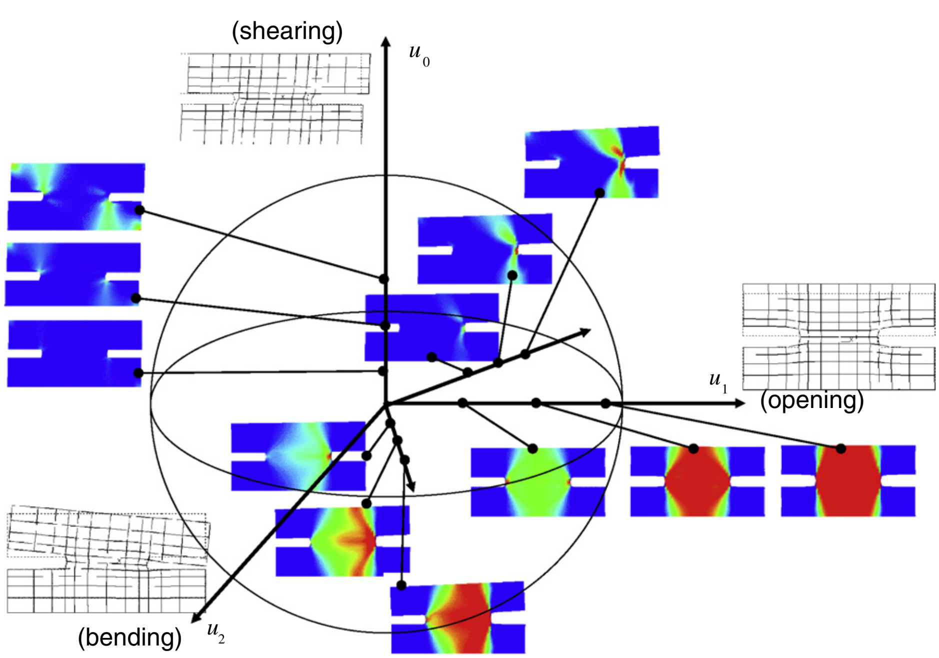

Fig. 11. DED distributions on the actual specimen used for the material characterization along characteristic points on representative paths of the loading subspace (u_1, u_2, u_6).

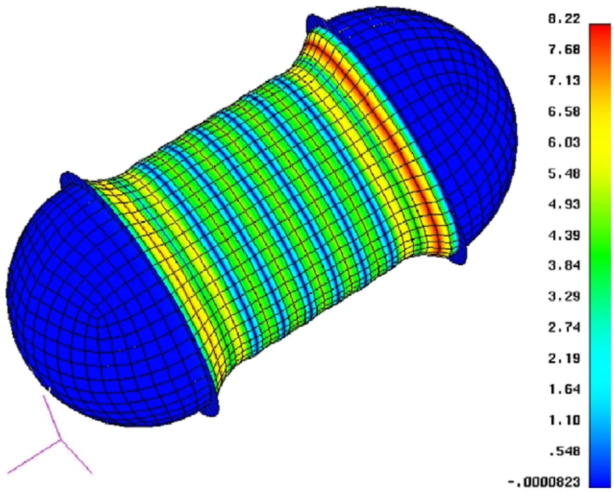

Fig. 12. Distribution of DED for an underwater ring-stiffened composite pressure vessel with steel semi-spherical end-caps under hydrostatic pressure.

shows distributions of the DED for a ring-stiffened cylindrical composite pressure vessel with semi-spherical end-caps.

Fig. 12 shows the axisymmetric softening behavior of the same vessel under hydrostatic pressure induced by underwater conditions. The hot spot zones clearly predict failures at the locations of the inflection area induced from the stiffness mismatch between the cylinder and the end-caps, which coincides with experimental observations. Another common characteristic is the strengthening effect of the ring-stiffeners that keep strain levels low and therefore low levels of DED. These images have been created by the visualization resources behind the computational models created in early versions of the computational infrastructure [24,25] that lead to the development of a special problem solving environment [27].

7. Conclusions

The evolution of 6-DoF mechatronically-based loading systems along with the corresponding computationally automated methodology has been described for the case of determining the constitutive behavior of composite materials by the use of the DEDF.

The systemic black and gray box descriptions of a material/structural system have been given along with its inverse problem setting. The determination of DEDF as the holder of the constitutive response of the composite material has been outlined as an optimization problem.

Representative applications of the use of DEDF have been provided as evidence of the power of this approach. The combination of mechatronic automation with the ever evolving computational technology provides a unique opportunity for reliably characterizing material systems and accurately simulating behavioral aspects of structural systems consisting of these materials. Knowing the non-linear constitutive behavior of a composite material system enables researchers and designers to employ the concept of DEDF for building mission critical failure theories based purely on the energetic considerations of failure.

This is ongoing work and involves a combination of robotic engineering, experimental mechanics and computational modeling.

Acknowledgement

The authors acknowledge the support by the Office of Naval Research, the National Science Foundation under Grant 0540419 and by NRL's 6.1 core-program.

References

[1] Factory PR. Effects of computational technology on composite materials research: the case of the dissipated energy density. In: Proceedings of the first hellenic conference on composite materials and structures, Democritus University of Thrace, Greece, July 2–5,1997, Thessaloniki: Kyriakidis Brothers S.A. Publishing House; 1997. p. 465–94.

[2] Michopoulos J. Computational and mechatronic automation of multiphysics research for structural and material systems. In: Recent advances in composite materials. Kluwer Academic Publishing; 2003. p. 9–21.

[3] Michopoulos J. Mechatronically automated characterization of material constitutive response. In: Proceedings of the 6th world congress on computational mechanics (WCCM-VI), September 5–10 2004, Beijing China: Tsinghua University Press and Springer; 2004. p. 486–91.

[4] Sebek ML, Braun AA. The evolution of testing equipment used in fracture mecahnics research, MTS monograph, Minneapolis (MN); 1994.

[5] Mast PW, Nash GE, Michopoulos JG, Thomas R, Badaliance R, Wolock I. Characterization of strain-induced damage in composites based on the dissipated energy density. Theor Appl Fract Mech 1995;22:71–125.

[6] Thagard P. Computational philosophy of science. Cambridge (MA): MIT Press; 1988.

[7] Zeigler BP, Kim TG, Praehofer H. Theory of modeling and simulation. 2nd ed. New York: Academic; 2000.

[8] Chandrupatla TR, Belegundu AD. Introduction to finite elements in engineering; 1991, 1997, 2001.

[9] Belytschko T, Liu WK, Moran B. Nonlinear finite elements for continua and structures. New York: John Wiley and Sons; 2000.

[10] Fowler M, Scott K. UML distilled. 2nd ed. Boston: Addison-Wesley; 2000.

[11] Michopoulos JG, Furukawa T. Towards hierarchical design optimization for simultaneous material characterization and control of experiments. In: Dulikravich GS, Colaco MJ, Orlande HRB, Tanaka M, editors. Inverse problems, design and optimization symposium Miami, Florida,USA, April 16–18, 2007, IPDO; p. 325–32.

[12] Michopoulos JG, Furukawa T. Multi-level coupling of dynamic data-driven experimentation with material identification. In: Yong Shi, Dick van Albada G, Jack Dongarra Peter M.A. Sloot, editors. International conference on computational science (ICCS07), Lecture Notes in Computer Science No. 4487, 2007(1), Berlin: Springer-Verlag; 2007. p. 1180–8.

[13] Michopoulos JG, Furukawa T, Hermanson JC, Lambrakos SG. Simultaneous hierarchical and multi-level optimization for material characterization and design of experiments. In: Proceedings of IDETC/CIE 2007 ASME 2007, Paper DETC2007-35470, ASME, DVD ISBN 0-7918-3806-4.

[14] Mast PW, Nash GE, Michopoulos JG, Thomas R, Badaliance R, Wolock I. Characterization of strain-induced damage in composites based on the dissipated energy density: Part II – Composite specimens and naval structures. Int J Theor Appl Fract Mech 1995;22:97–114.

[15] Mast PW, Nash GE, Michopoulos JG, Thomas R, Badaliance R, Wolock I. Characterization of strain-induced damage in composites based on the dissipated energy density: Part III – General material constitutive relation. Int J Theor Appl Fract Mech 1995;22:115–25.

[16] Henderson DW. Experiencing geometry in euclidean, spherical, and hyperbolic spaces. Prentice-Hall; 2001.

[17] Krajcinovic D. Constitutive equations for damaging materials. J Appl Mech 1983;50:355–60.

[18] Kachanov L. Introduction to continuum damage mechanics. The Netherlands: Martinus Nijhoff Publishers; 1986.

[19] Lemaitre J, Chaboche J-L. Mechanics of solids. London: Cambridge University Press; 1990.

[20] Voyiadjis GZ, Park T. Anisotropic damage effect tensor for the symmetrization of the effective stress tensor. J Appl Mech 1997;64:106–10.

[21] Fletcher R. Practical methods of optimization. Wiley; 1993.

[22] Powell MJD. A fast algorithm for nonlinearly constrained optimization calculations. In: Numerical analysis, Dundee 1977, Lecture Notes in Mathematics 630, Springer; 1977.

[23] Gill PE, Murray W. Newton type methods for linearly constrained optimization. In: Gill PE, Murray W, editors. Numerical methods for constrained optimization. Academic Press; 1974.

[24] Michopoulos J, Badaliance R, Chwastyk T, Gause L, Mast P, Farhat C, Lesoinne M. Strain induced material nonlinearity for AGARD Wing 445.6 in a virtual wind tunnel environment: results from coupled multiphysics simulation, DoD HPC user group conference 2000, Albuquerque New Mexico; 2000.

[25] Michopoulos J, Farhat C, Lesoinne M, Mast P, Badaliance R, Chwastyk T, Gause L. Material softening issues in a multiphysics virtual wind tunnel environment, AIAA Paper 2002-1095. In: Proceedings of 40th aerospace sciences meeting and exhibit, January 14–17, Reno, Nevada; 2002.

[26] Michopoulos JG, Mast PW, Badaliance R, Wolock I. Health monitoring of smart structures by the use of dissipated energy. In: Carman GP, Garcia E, editors. ASME Proceedings of 93 WAM on adaptive structures and material systems, ASME, AD, vol. 35, 1993. p. 457–62.

[27] Michopoulos J, Tsompanopoulou P, Houstis E, Farhat C, Lesoinne M, Rice J, Joshi A. On a data driven environment for multiphysics applications. Future Generat Comput Syst J 2005;21(6):953–68.